Gaussian beam photothermal single particle microscopy

Markus Selmke, Marco Braun, and Frank Cichos*

University of Leipzig, Linnéstrasse 5, Leipzig 04103, Germany
**Corresponding author: cichos@uni-leipzig.de*

Received May 29, 2012; accepted August 31, 2012;
posted September 5, 2012 (Doc. ID 169548); published September 28, 2012

We explore the intuitive lensing picture of laser-heated nanoparticles occurring in single particle photothermal (PT) microscopy. The effective focal length of the thermal lens (TL) is derived from a ray-optics treatment and used to transform the probing focused Gaussian beam with ABCD Gaussian matrix optics. The relative PT signal is obtained from the relative beam-waist change far from the TL. The analytical expression is semiquantitative, capable of describing the entire phenomenology of single particle PT microscopy, and shows that the signal is the product of the point-spread functions of the involved lasers times a linear function of the axial coordinate. The presented particularly simple and intuitive Gaussian beam lensing picture compares favorably to the experimental results for 60 nm gold nanoparticles and provides the prescription for optimum setup calibration.

OCIS codes: 070.2590, 190.4870, 110.6820.

1. INTRODUCTION

Absorbing nanoparticles too small to be detected by scattering or direct absorption may be imaged by photothermal (PT) microscopy. The method's superior sensitivity rests on the fact that it uses the absorption of light, which decreases only with the volume of the particles in contrast to light scattering, which decreases with the volume squared for small particles [1]. As an ever more popular tool, this technique has been used to study nanocrystals [2], carbon nanotubes [3], and single molecules [4] through their absorption. Thereby, absorption cross sections of fixed particles were extracted [5] or mobilities of (heated) solute particles [6,7] were attained through PT correlation spectroscopy [8,9]. An early developed theory in a scattering framework [10] was incomplete and did not account for the axial shape and magnitude of the signal. In fact, the PT signal in single particle microscopy is dual lobed and thereby comprehensible as a lensing phenomenon. While this complex generalized Mie scattering framework quantitatively described the situation [11], the physics of the lensing action remained hidden in the laborious computations of the scattering and beam shape coefficients. Similar to the thin sample slab PT spectroscopy [12] ABCD framework by Moreau and Loriette [13], we hereby present a minimal semiquantitative and intuitive Gaussian beam transformation model of single particle PT microscopy.

PT single particle microscopy is a sample-scanning method that uses two coaxial focused laser beams: a resonant heating beam to generate the medium's refractive index perturbation through the nanoparticle's absorption of electromagnetic energy and a nonresonant detection laser, which is transmitted through the sample. The modulation amplitude of the detected power induced by a modulation of the heating laser is detected by a photodiode. Normalization to the transmitted power P_0 when the heating laser is off defines the relative PT signal,

$$\Phi = (P_{\mathrm{th}} - P_0)/P_0. \tag{1}$$

To describe the action of a local refractive index perturbation generated by a heated nanoparticle on the propagation of the probing Gaussian beam in the framework of ABCD matrix optics [14], one first needs to derive a ray-optics transfer matrix for the system. We have recently shown that the signal in PT single particle microscopy can be understood in terms of the action of a nanolens. We therefore expect that this lensing action can be represented by a transfer matrix M_f corresponding to a (thermal) lens. Section 2 will derive the effective focal length of this thermal lens (TL). Subsequently, the quantitative relative PT signal is computed in the ABCD framework. The found analytical expression will then be compared to measurements on a single gold nanoparticle (AuNP).

2. THEORY

A. Focal Length of the TL

The focal length of the continuous refractive index perturbation around a heated nanoparticle can be obtained by considering Fermat's principle. In geometrical optics, Fermat's variation principle describes the path of an optical ray of light in an inhomogeneous refractive index field $n(\mathbf{r})$ and reads in its differential form [15]:

$$\mathbf{r}'' = \nabla\left(\frac{1}{2}n^2(\mathbf{r})\right), \qquad |\mathbf{r}'| = n(\mathbf{r}), \tag{2}$$

where the prime $' = d/ds$ denotes a derivative with respect to the path coordinate s. In the case of interest here, a spherically symmetric refractive index profile $n(r)$ will originate from the release of heat from an absorbing nanoparticle. It is specified by its contrast Δn and the particle radius R characterizing the distance from the particle at which the perturbation is decreased to half: $n(\mathbf{r}) = n_0 + \Delta n R/r$ with $\Delta n = \Delta T[dn/dT]$. The induced particle temperature increment ΔT is determined by the power P_{abs} absorbed by the nanoparticle and the materials' thermal conductivity κ through $\Delta T =$

$P_{\mathrm{abs}}/[4\pi\kappa R]$. Therefore, the refractive index contrast Δn corresponds to

$$\Delta n = \left[\frac{dn}{dT}\right]\frac{P_{\mathrm{abs}}}{4\pi\kappa R}. \tag{3}$$

The amount of power P_{abs} absorbed by the particle depends on its absorption cross section σ_{abs} at the heating laser wavelength λ_h and the heating beam's intensity I_h at the nanoparticle position via $P_{\mathrm{abs}} = \sigma_{\mathrm{abs}} I_h$.

The solution to the differential Eq. (2) with the given type of refractive index profile is the ray equation. In polar coordinates, we obtain, in analogy to the perturbed Kepler problem [16], Eq. (4),

$$r(\phi, b) = \frac{p}{\epsilon\,\cos\left(\gamma[\phi - \phi_0]\right) - 1}. \tag{4}$$

This equation describes trajectories for rays that approach parallel and at a distance $b > 0$ to the optical axis, as illustrated in Fig. 1 for $\Delta n < 0$. The angle of closest approach ϕ_0, the perturbation parameter γ, the eccentricity ϵ, and the normalized semilatus rectum p/b depend on the inverse strength ξ and the incident height b through the dimensionless quantity $b\xi$; see Eq. (5). Thus, the trajectories are completely determined by the value of ξ^{-1}, as defined in Eq. (5). Mathematically, they represent weakly perturbed hyperbolic trajectories with the particle being the exterior ($\xi > 0$) or interior ($\xi < 0$) focus [17]:

$$\left.\begin{aligned} \xi &= -n_0/R\Delta n \\ p &= (b^2\xi^2 - 1)/\xi \\ \gamma^2 &= 1 - b^{-2}\xi^{-2} \\ \epsilon &= b\xi \\ \phi_0 &= \pi - \gamma^{-1}\,\arccos\,(1/\epsilon) \\ &\approx \pi/2 + b^{-1}\xi^{-1} + \mathcal{O}(b^{-2}\xi^{-2}) \end{aligned}\right\}. \tag{5}$$

The quantity $|b\xi| > |n_0/\Delta n| \gg 1$ is a large number, since the impact parameter b is bound to be larger than the particle radius R, and the induced refractive index contrast $\Delta n = \mathcal{O}(10^{-3})$ is always much smaller than the unperturbed refractive index n_0, which is of the order of unity. While the asymptote to the ray solution Eq. (4) for $\phi \to \pi$ is a horizontal line at height b describing an undeflected straight ray, the other asymptote at $\phi \to 2\,\phi_0 - \pi$ permits the extraction of a focal length (white lines in Fig. 1). The calculation yields $f\xi = -b\xi/\sin(2\,\arccos(b^{-1}\xi^{-1})/\gamma)$, such that $f\xi \approx -b^2\xi^2/2$, where smaller terms of order $\mathcal{O}(b\xi)$ have been omitted. The focal length of the TL, Eq. (6),

$$f(b) \approx b^2 n_0/[2\Delta n R], \tag{6}$$

is thus seen to vary quadratically with the impact parameter b and even to diverge as b grows large. It exhibits spherical aberrations. However, as a focused probing laser beam of finite extent is incident onto the lens, large impact parameters will not be realized. For a Gaussian beam with waist ω_0 and spreading length $2z_R = 2\pi n_0\omega_0^2/\lambda$ [14] located at a distance z_p relative to the position of the TL, an effective focal length f_{eff} is expected. It will involve an effective squared impact parameter b_{eff}^2, which depends on the profile of the beam at the lens. A weighting of b^2 by the Gaussian intensity profile $I_d(b, z_p)$ of the probing Gaussian beam defines such a weighted quantity. The result, $b_{\mathrm{eff}}^2(z_p) = \omega_0^2[z_p^2/z_R^2 + 1]/2$, is half the square of the beam waist size at the position of the lens. The focal length, Eq. (6), of the TL for such an offset Gaussian beam then becomes

$$f_{\mathrm{eff}}(z_p) \approx \frac{n_0}{\Delta n}\frac{\omega_0^2}{4R}\left[\frac{z_p^2}{z_R^2} + 1\right]. \tag{7}$$

The strength of the TL as experienced by the probing beam is inversely proportional to the focal length and thus directly proportional to the refractive index contrast Δn. In an experiment the absorbed power $P_{\mathrm{abs}}(z_p)$ provided by the focused heating beam will induce this contrast [see Eq. (3)] and may thus also depend on the axial position. A negative focal length is obtained for a negative thermorefractive coefficient and signifies a divergent lens. A convergent lens will be obtained for materials that show a positive change in their refractive index with temperature. This is the case, for example, for some liquid crystals. Equation (7) now also includes the circumstance that, for large offsets z_p, the average impact parameter seen becomes large and the lens acting on the whole beam thereby becomes weak. In the ray-optics treatment of thin lenses, one finds that the incident ray height above the optical axis remains unaffected by the lens and only the ray angle is changed. Similarly, here we find for the intersection height y_0 of the asymptote with the vertical axis $y_0/b \approx 1 + 2b^{-2}\xi^{-2} + \mathcal{O}(b^{-3}\xi^{-3})$, such that typically $y_0 \approx b$, which is the thin lens assumption. We may therefore proceed with a matrix optics formalism describing the modification of the propagation of the probing laser beam as induced by a thin lens of focal length f_{eff}.

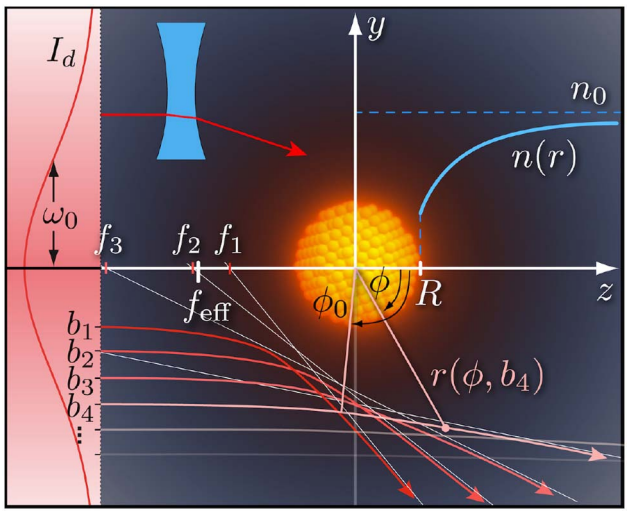

Fig. 1. (Color online) Heated nanoparticle creates a refractive index profile $n(r)$, which constitutes the thermal lens. A ray-optics treatment delivers a focal length when probed by a confined Gaussian beam (see text). For typical material parameters, the focal lengths are large as compared to the particle dimension, i.e., $f \gg R$.

B. ABCD Gaussian Matrix Optics

The transformation of a Gaussian beam by an optical element can be described by a matrix [14] acting on a vector $\{q_{\mathrm{in}}, 1\}^{\mathrm{T}}$. The parameter q describes the Gaussian beam at a certain position along the optical axis and is a function of the radius of curvature R_C and the beam waist ω, as defined in Eq. (8).

The beam transfer matrices characterize the optical elements that the beam passes and may be concatenated if the beam passes a series of elements. The matrices are 2×2 ray-transfer matrices $M = \{A, B; C, D\}$, and the ABCD law for Gaussian beams transforms an input beam described by q_{in} to and output beam characterized by q_{out}:

$$q_{\text{in}}^{-1} = \frac{1}{R_C(z_p)} - i\frac{\lambda/n}{\pi\omega^2(z_p)}, \qquad q_{\text{out}} = \frac{Aq_{\text{in}} + B}{Cq_{\text{in}} + D}. \tag{8}$$

In PT single particle microscopy, the TL is periodically switched on and off. Thus, the probe beam is either influenced by the TL or not. Consequently, two sets of ray transfer matrices are required to describe the PT signal. Both include the sample interface and free space propagation for a distance d as depicted in Fig. 2. According to this scheme, we use $M_{\text{th}} = M_d M_i M_f$ in the case where the TL is present and $M_0 = M_d M_i$ in the case when it is switched off. The individual transfer matrices [14] are $M_d = \{1, d; 0, 1\}$ for free space propagation by a distance d, $M_f = \{1, 0; -1/f, 1\}$ for a thin lens of focal length f, and $M_i = \{1, 0; 1, n_0/n_1\}$ for the refraction by a flat dielectric interface from n_0 to n_1. The output beam parameter q_{out} then encodes the transformed beam shape in its real and imaginary part. For instance, the beam waist is related to the imaginary part via $\omega^2 = -\lambda/[n\pi\text{Im}(q_{\text{out}}^{-1})]$.

C. Relative PT Signal

As mentioned earlier, the relative PT signal is the ratio of the detected power change due to the TL to the detected power without a TL [Eq. (1)]. On the optical axes, this translates into a ratio of intensities, $\Phi = (I_{\text{th}} - I_0)/I_0$. For a Gaussian beam, the intensity is proportional to its inverse beam waist squared, $I \propto \omega^{-2}$. The ABCD matrix optics law provides the necessary beam waists behind the sample. Then, the relative PT signal simplifies in the far field and weak lens limit, where $d \gg \{f, z_R\}$ and $f \gg z_R$, respectively, to

$$\Phi(z_p) = 2z_p/f. \tag{9}$$

As signified by the signal's proportionality to z_p, the probing beam offset with respect to the lens determines whether the beam is collimated or further diverged, yielding a positive or negative relative PT signal, respectively. The behavior is reversed if the sign of the focal length changes. The relative PT signal is also inversely proportional to the focal length. This simply means that weak lenses, which have a large focal length, modify the probing beam to a smaller extent. The interface parameters $\{n_0, n_1\}$ do not appear in Eq. (9) as the sample/air interface affects both the nonlensed as well as the lensed beam in an equivalent manner. Substitution of $f \to f_{\text{eff}}$ Eq. (7) into Eq. (9) yields the axial relative PT signal dependence. However, as the absorbed power $P_{\text{abs}}(z_p) = \sigma_{\text{abs}} I_h(z_p)$ controls the strength $\Delta n(z_p)$ of the lens [see Eq. (3)], one needs to include the axial intensity profile of the heating beam in the considerations. For a Gaussian heating beam, the axial intensity profile $I_h(z_p)$ is a Lorentzian with a maximum intensity $I_0 = 2P_h/\pi\omega_{0,h}^2$ [14] determined by its beam waist $\omega_{0,h}$ and its total power P_h. This maximum is typically shifted with respect to the detection beam by some axial offset Δz_f; see Fig. 3 (top). Combining the expression for the absorbed power, Eqs. (3), (7), and (9), the relative PT signal as a function of the particle to probe beam offset z_p reads

$$\Phi = \frac{4P_h\sigma_{\text{abs}}\left[\frac{dn}{dT}\right]}{\pi^2\kappa n_0\omega_{0,h}^2\omega_0^2}\left[\frac{(z_p - \Delta z_f)^2}{z_{R,h}^2} + 1\right]^{-1} z_p\left[\frac{z_p^2}{z_R^2} + 1\right]^{-1}. \tag{10}$$

The relative PT signal according to this formula is depicted in Fig. 3 as a function of z_p at various defocusing Δz_f. The signal correctly accounts for the experimentally observed control of the two oppositely signed peaks. While the lensing, and thereby the sign of the signal, is always determined by the probing beam position z_p relative to the lens [Eq. (9)], the magnitude of the signal is also controllable by the axial position of the heating beam. This result is formally very similar to Moreau and Loriette's result [13] for thin films. The PT signals' proportionality to dn/dT and the absorbers volume is immediately recovered [10], considering that, for small particles, $\sigma_{\text{abs}} \propto R^3$ [1]. Also, the functional form reveals that the signal is proportional to the product of the point-spread functions and a linear function for the Gaussian beam case, i.e., $\Phi \propto I_h I_d z_p$. For highly focused beams, we have experimentally shown

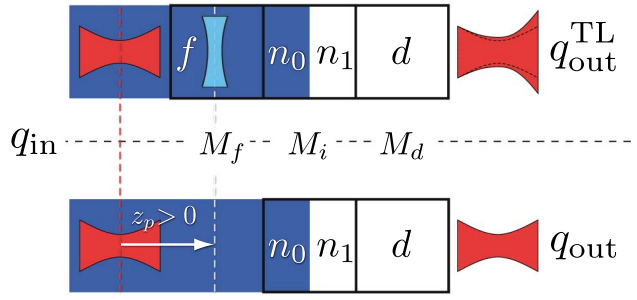

Fig. 2. (Color online) Probing Gaussian beam is focused at a distance z_p to the lens (first optical element). An interface from a medium with refractive index n_0 to air with n_1 and free space propagation by a distance d follow. (Top) Beam transformation through the optical system with a lens present. (Bottom) Beam transformation without the lens.

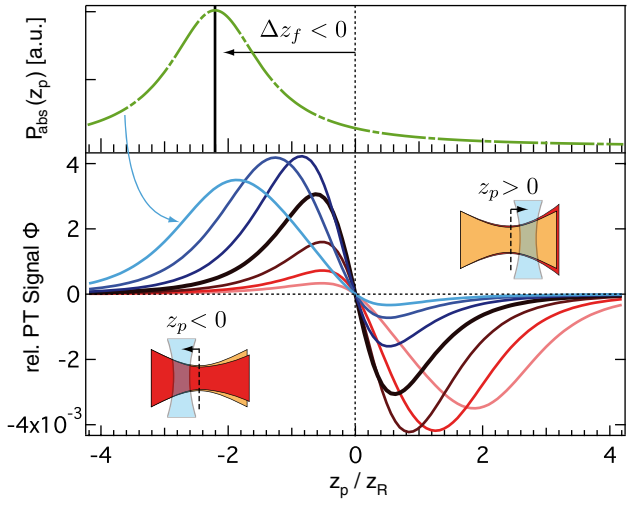

Fig. 3. (Color online) (Top) Lorentzian profile of the power $P_{\text{abs}}(z_p)$ absorbed by the particle for an axial laser offset $\Delta z_f = -2.1 z_R$. (Bottom) Axial scans of the relative PT signal, Eq. (10) ($\times F$), for $\Delta z_f/z_R = \{-2.1, -1.4, -0.7, 0.7, 1.4, 2.1\}$ (blue to red). Parameters: $R = 30$ nm, $\Delta T = 200$ K corresponding to the experimental parameters $\omega_{0,h} = 0.380$ μm, $\omega_0 = 0.315$ μm, $\sigma_{\text{abs}}(\lambda_h) = 1.16 \times 10^{-14}\,\text{m}^2$, and $P_h = 225$ μW.

[11,18] $\Phi(z_p) \propto \exp(-2z^2/\omega_z^2)[z - z_0]$ with an axial signal width ω_z to be a good approximation to the signal. This approximation, too, is of the form of a product of two offset point-spread functions (PSFs, axial Gaussians in this case) times z_p if the axial beam waists of the individual beams are assumed equal. Numerically, it follows from Eq. (10) that, in order to obtain the maximum signal from the TL, the lasers should be offset by about one Rayleigh range, i.e., $\Delta z_f \approx \pm z_R$. Already from the previous discussion, it is clear that both positive and negative signals will be experimentally observable as in early PT correlation spectroscopy experiments [9]. The new foundation given above now opens the way to control the shape of the PT signal for new applications such as twin-focus PT correlation spectroscopy (Twin-PhoCS), which will be detailed in a forthcoming paper [18]. Since we have used the beam waist to define an intensity, the current model only describes the relative PT signal on axis at zero numerical detection aperture. However, as we have shown recently [11,19], the relative PT signal depends on the collection angle domain. As all experiments are carried out with a finite collection angle domain, one needs to include a correction factor $F = \Phi(\theta)/\Phi(0)$ to the above-described PT signal, where $\Phi(\theta)$ is the PT signal for a certain detection angle θ. This factor can be simply obtained from the extrapolation of an aperture-diameter-dependent PT signal measurement or from more elaborate models [11,19] [see Fig. 5(d) below, markers and solid line, respectively]. The aperture-dependent measurement reveals a factor of $F = 0.1$ in Eq. (10) to account for the used finite numerical aperture of NA = 0.8 (see Section 3).

3. EXPERIMENTAL REALIZATION

To validate the theoretical predictions, we have performed PT measurements on single AuNPs of radius $R = 30$ nm with focused Gaussian heating and detection beams. Therefore, the particles were embedded in a polymer film (PDMS) of about $d = 30$ μm thickness and the sample axially moved through the foci with an AuNP on the optical axis. To experimentally realize focused Gaussian heating and probing beams, we have underfilled the back aperture of the illuminating microscope objective (oil immersion, 100x, NA = 1.4). The homebuilt sample-scanning microscope is described in detail in [11]. The two lasers focused on the sample are collected with a NA = 0.8 dry objective behind the sample and imaged onto two photodiodes after passing appropriate filters. We have modeled the recorded transmitted powers within the generalized Lorenz–Mie theory (GLMT) [20] using Gaussian beam shape coefficients [21] and our finite collection angle extension [11]. The agreement seen in Fig. 4 between experiment and calculation validates the assumption of Gaussian beams and yields $z_R = 0.717$ μm, $\omega_0 = 0.315$ μm. Further, the offset of the scatter-image dips Δz_{sca} may be translated into the Gaussian beam offset with the calculation (Fig. 4, graphs) via $\Delta z_f = \Delta z_{\mathrm{sca}} + 0.387$ μm. The rather large radius of the AuNPs, $R = 30$ nm, has been chosen to still allow for this parameter extraction. Alternatively, the weak fluorescence of AuNPs may be used to extract Δz_f by measuring the fluorescence peak offset relative to the zero crossing of the PT signal [22]. Figure 5 displays the obtained axial relative PT signal scans. Depending on the offset Δz_f of the heating beam relative to the detection beam, either the positive signal lobe or the negative lobe is enhanced. Equation (10) predicts this

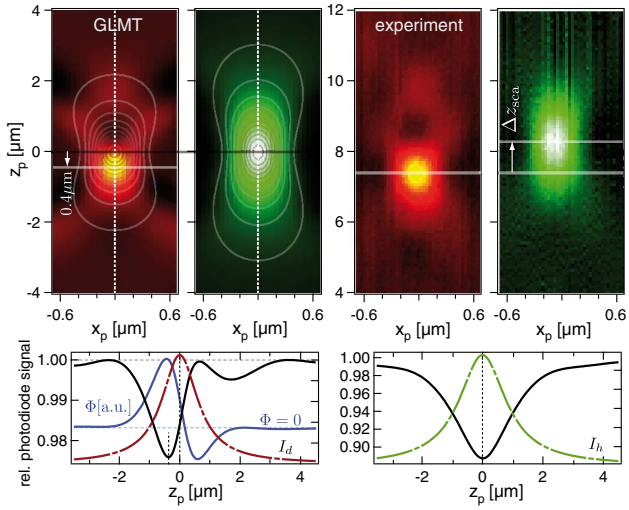

Fig. 4. (Color online) (Top) The left two images show theoretical $R = 30$ nm AuNP xz scans of transmitted powers computed within GLMT (probing, $\lambda = 0.635$ μm, $\omega_0 = 0.315$ μm; heating beam, $\lambda_h = 0.532$ μm, $\omega_{0,h} = 0.330$ μm; both in PDMS $n_0 = 1.46$). The left and right contours show incident intensities I_d and I_h, respectively. The right two images show the corresponding scans recorded with a photodiode. (Bottom) Theoretical axial scans (black, along white dashed lines) and $\Phi(z_p)$ for $\Delta z_f = 0$ (blue; gray solid in print). Also shown are the axial Lorentzian heating beam profiles (in arbitrary units, solid-dashed, colored).

effect nicely as shown by the solid lines in the bottom row plots. Since the particle used is still scattering and since its scattering cross section σ_{sca} senses its embedding refractive index, the PT signal does not vanish at $\Delta z_f = 0$ [11]. To account for this additional effect, the Δz_f axis has been shifted by the offset of the particle to the signal zero crossing, i.e., by 0.17 μm. Now, experiment (markers) and theory (lines) match nicely, demonstrating the possibility to even extract induced particle temperatures or absorption cross sections σ_{abs} quantitatively. We attribute the remaining discrepancy at large

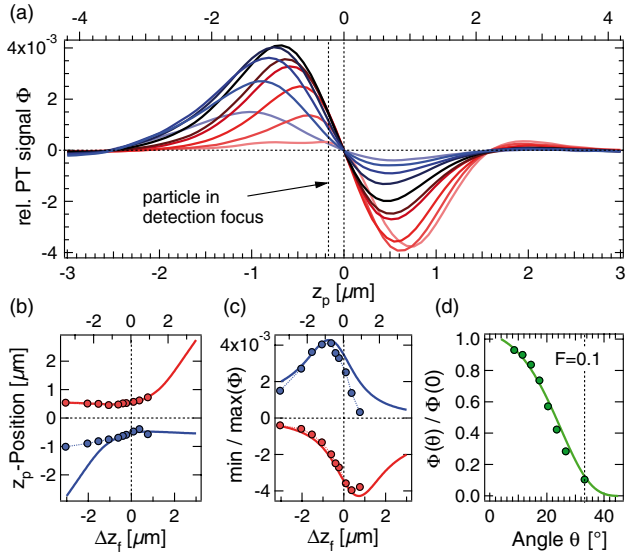

Fig. 5. (Color online) (a) Experimental axial signal scans $\Phi(z_p)$. (b) Extrema positions versus axial displacement of heating and detection foci. (c) Extrema values of relative PT signal. (d) Dependence of the finite angle correction factor $F = \Phi(\theta)/\Phi(0)$ on the numerical aperture NA $= n_0 \sin(\theta)$ at $z_p = -0.5$ μm. Parameters as in Fig. 3. Top axes for axial coordinates have been scaled by z_R.

relative laser offsets $\Delta z_f/z_R > 1$ [see Figs. 5(b) and 5(c)] to the fact that the heating beam was in fact weakly aberrated, which can be also seen by the small additional lobe at $z_p \approx 2.0$ μm in Fig. 5(a). Remaining aberration peaks in the PSF explain the deviating PT signal shape for negative z_p and large negative laser offsets Δz_f. Further, since Δz_f was adjusted by changing the heating beam divergence in front of the focusing microscope objective, the overfilling and thereby the beam waist in the focal region changed slightly for the heating beam: $\omega_{0,h} = 0.321\ \mu\text{m} - 0.045\Delta z_f$. The maximum signal was obtained when the lasers were offset by about one Rayleigh range, i.e., $\Delta z_f \approx \pm z_R$ [see Fig. 5(c), top axis], which was already predicted by Eq. (10).

4. CONCLUSIONS

We have shown that the relative PT signal shape can be modeled by the action of a TL in the framework of ABCD Gaussian transformation optics. The resulting expression reveals that it is the product of the involved laser's PSFs times the axial coordinate. This means that, quite universally, for any focused beam probing the TL, both positive and negative signals are to be expected [9] and their relative amplitude is adjustable by the two laser's offset. The analytical expression derived here, Eq. (10), is validated experimentally for Gaussian beams. Our results may be used to conveniently extract absorption cross sections from PT measurements and provide a guideline for the relative focus adjustment of the probing and heating laser beams.

ACKNOWLEDGMENTS

We thank D. Rings and K. Kroy for helpful discussions. Financial support by the Deutsche Forschungsgemeinschaft (DFG) research unit 877 and the graduate school BuildMoNa, as well as funding by the European Union and the Free State of Saxony, is acknowledged.

REFERENCES

1. C. F. Bohren and D. R. Huffman, *Absorption and Scattering of Light by Small Particles* (Wiley-VCH, 1998).
2. S. Berciaud, L. Cognet, G. Blab, and B. Lounis, "Photothermal heterodyne imaging of individual nonfluorescent nanoclusters and nanocrystals," Phys. Rev. Lett. **93**, 257402 (2004).
3. S. Berciaud, L. Cognet, and B. Lounis, "Luminescence decay and the absorption cross section of individual single-walled carbon nanotubes," Phys. Rev. Lett. **101**, 077402 (2008).
4. A. Gaiduk, M. Yorulmaz, P. V. Ruijgrok, and M. Orrit, "Room-temperature detection of a single molecule's absorption by photothermal contrast," Science **330**, 353–356 (2010).
5. S. Berciaud, L. Cognet, and B. Lounis, "Photothermal absorption spectroscopy of individual semiconductor nanocrystals," Nano Lett. **5**, 2160–2163 (2005).
6. D. Rings, R. Schachoff, M. Selmke, F. Cichos, and K. Kroy, "Hot Brownian motion," Phys. Rev. Lett. **105**, 090604 (2010).
7. D. Rings, M. Selmke, F. Cichos, and K. Kroy, "Theory of hot Brownian motion," Soft Matter **7**, 3441–3452 (2011).
8. R. Radünz, D. Rings, K. Kroy, and F. Cichos, "Hot Brownian particles and photothermal correlation spectroscopy," J. Phys. Chem. A **113**, 1674–1677 (2009).
9. P. M. R. Paulo, A. Gaiduk, F. Kulzer, S. F. G. Krens, H. P. Spaink, T. Schmidt, and M. Orrit, "Photothermal correlation spectroscopy of gold nanoparticles in solution," J. Phys. Chem. C **113**, 11451–11457 (2009).
10. S. Berciaud, D. Lasne, G. Blab, L. Cognet, and B. Lounis, "Photothermal heterodyne imaging of individual metallic nanoparticles: theory versus experiment," Phys. Rev. B **73**, 045424 (2006).
11. M. Selmke, M. Braun, and F. Cichos, "Photothermal single particle microscopy, detection of a nano-lens," ACS Nano **6**, 2741–2749 (2012).
12. S. Bialcowski, *Photothermal Spectroscopy Methods for Chemical Analysis* (Wiley, 1996).
13. J. Moreau and V. Loriette, "Confocal dual-beam thermal-lens microscope: model and experimental results," Jpn. J. Appl. Phys. **1**, 7141–7151 (2006).
14. B. E. A. Saleh and M. C. Teich, *Fundamentals of Photonics*, Wiley Series in Pure and Applied Optics (Wiley, 1991).
15. J. Evans and M. Rosenquist "'$F = ma$' optics," Am. J. Phys. **54**, 876–883 (1986).
16. J. Sivardière, "Perturbed elliptic motion," Eur. J. Phys. **7**, 283–286 (1986).
17. A. A. Rangwala, V. H. Kulkarni, and A. A. Rindani, "Laplace Runge Lenz vector for a light ray trajectory in r^{-1} media," Am. J. Phys. **69**, 803–809 (2001).
18. M. Selmke, R. Schachoff, M. Braun, and F. Cichos, "Twin-focus photothermal correlation spectroscopy," RSC Adv. (submitted).
19. M. Selmke, M. Braun, and F. Cichos, "Nano-lens diffraction around a single heated nano particle," Opt. Express **20**, 8055–8070 (2012).
20. G. Gouesbet, B. Maheu, and G. Gréhan, "Light-scattering from a sphere arbitrarily located in a Gaussian beam, using a Bromwich formulation," J. Opt. Soc. Am. A **5**, 1427–1443 (1988).
21. K. Ren, G. Gréhan, and G. Gouesbet, "Localized approximation of generalized Lorenz Mie theory: faster algorithm for computations of beam shape coefficients, g_n^m," Part. Part. Syst. Charact. **9**, 144–150 (1992).
22. A. Gaiduk, P. V. Ruijgrok, M. Yorulmaz, and M. Orrit, "Making gold nanoparticles fluorescent for simultaneous absorption and fluorescence detection on the single particle level," Phys. Chem. Chem. Phys. **13**, 149–153 (2011).